# One-dimensional discrete aggregation-fragmentation model

N. Zh. Bunzarova,[1,2] N. C. Pesheva,[2,*] and J. G. Brankov[1,2]
[1]*Bogoliubov Laboratory of Theoretical Physics, Joint Institute for Nuclear Research, 141980 Dubna, Russia*
[2]*Institute of Mechanics, Bulgarian Academy of Sciences, 1113 Sofia, Bulgaria*

(Received 19 April 2019; published 30 August 2019)

We study here one-dimensional model of aggregation and fragmentation of clusters of particles obeying the stochastic discrete-time kinetics of the generalized totally asymmetric simple exclusion process (gTASEP) on open chains. The gTASEP is essentially the ordinary TASEP with backward-ordered sequential update (BSU), however, equipped with two hopping probabilities: $p$ and $p_m$. The second modified probability $p_m$ models a special kinematic interaction between the particles of a cluster in addition to the simple hard-core exclusion interaction, existing in the ordinary TASEP. We focus on the nonequilibrium stationary properties of the gTASEP in the generic case of attraction between the particles of a cluster. In this case the particles of a cluster have higher chance to stay together than to split, thus producing higher throughput in the system. We explain how the topology of the phase diagram in the case of irreversible aggregation, occurring when the modified probability equals unity, changes sharply to the one, corresponding to the ordinary TASEP with BSU, as soon as the modified probability becomes less than unity and aggregation-fragmentation of clusters appears. We estimate various physical quantities in the system and determine the parameter-dependent injection and ejection critical values by extensive computer simulations. With the aid of random walk theory, supported by the Monte Carlo simulations, the properties of the phase transitions between the three stationary phases are assessed.

DOI: 10.1103/PhysRevE.100.022145

## I. INTRODUCTION

The asymmetric simple exclusion process (ASEP) is one of the simplest models of self-driven many-particle systems with bulk particle-conserving stochastic dynamics exhibiting phase transitions in nonequilibrium steady state. In the extremely asymmetric case, when particles are allowed to move in one direction only, it reduces to the totally ASEP (TASEP). These models are some of the rare examples of exactly solved models far from equilibrium (see Refs. [1–3]). Presently, our understanding of non-equilibrium systems lags behind our knowledge of equilibrium systems and ASEP and TASEP are considered paradigmatic models (similarly to the Ising model in the equilibrium case) for understanding a variety of properties of systems in nonequilibrium steady states, nonequilibrium phase transitions and various phenomena with no counterpart in the equilibrium case. Different variants of TASEP model are widely studied currently, since it is believed that this model can be helpful in understanding various types of systems in Nature, such as kinetics of protein synthesis [4,5], molecular motors on a single track [6], colloid particles moving in narrow channels [7–9], and vehicles on a single-lane road [10–13], etc. In the model under consideration here, the particles obey the dynamics of the generalized TASEP (gTASEP) [14], which is the ordinary TASEP with backward-sequential update (BSU), however, having two hopping probabilities: $p$ and $p_m$. The modified probability $p_m$ models a special kinematic interaction between the particles in a cluster (which hop during the same integer-time moment) in addition to the simple hard-core exclusion interaction, existing in ordinary TASEP. In principle, the model admits the study of aggregation-fragmentation phenomena, fluctuations and finite-size effects in nonequilibrium stationary states induced by the boundary conditions.

We remind the reader that the original TASEP was defined as a continuous-time Markov process (random-sequential update in the Monte Carlo simulations) and was solved exactly with the aid of recurrence relations by Domany *et al.* [15] for special values of the model parameters, and by Schütz and Domany [16] in the general case. A breakthrough in the methods for solving TASEP on open chains marks the matrix-product representation of the steady-state probability distribution, found in Ref. [17]. Different versions of this approach, known as the Matrix Product Ansatz (MPA), were used also to obtain exact solutions for the stationary states of TASEP and ASEP under several types of discrete-time stochastic dynamics: sublattice-parallel [18,19], forward-ordered and backward-ordered sequential [20,21], and fully parallel (simultaneous updating of all sites) [22,23]. One of the goals of these studies was also to see how the system dynamics (update rules) influences the system nonequilibrium steady-state properties. An extensive comparative study of the ASEP with different updates was presented in Ref. [24] with the aim for a better understanding of the similarities and differences of the different updates. It appeared that they all have the same structure of the phase diagram and relations were established connecting the current and bulk density in ASEPs with different updates. The above studied cases of TASEP show also that the only dynamics that allow clusters to move forward as a whole entity is the backward-ordered one. Then, the probability for translation of a cluster of $k$ particles one site

*Corresponding author: nina@imbm.bas.bg

 

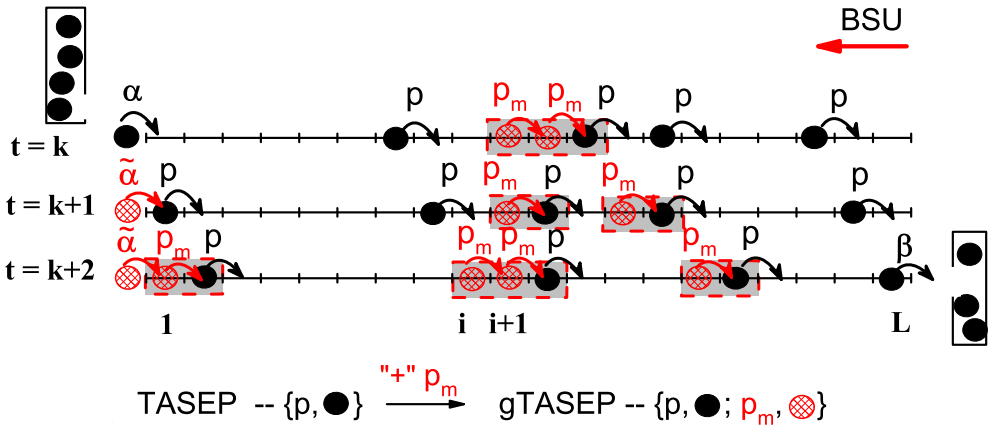


FIG. 1. Schematic image of the generalized TASEP, showing the time evolution of system configuration at three consecutive time steps. Isolated particles and the first particle of a cluster (shown as gray boxes) on the right (head particle) are shown with black solid circles—they may move one site to the right with probability $p$. Particles, which belong to a cluster (except the head particle), are shown with patterned (red) circles—they may move one site to the right (provided the particle in front of them has moved at the same time step) with a modified probability $p_m$. When $p_m > p$ ("attraction" interaction) the particles have higher probability to stay in clusters than to split. The left boundary condition is also modified accordingly to ensure consistency with the update rules in the bulk (for more details see the text).

to the right is $p^k$, while such a cluster is broken into two parts with probability $p - p^k$. That is why gTASEP is based upon TASEP with BSU. Under the generalized TASEP dynamics, the probability for translation of a cluster of $k$ particles one site to the right becomes $pp_m^{k-1}$, and its fragmentation into two parts happens with probability $p(1 - p_m^{k-1})$.

In terms of real traffic the case $p_m > p$ (termed "attraction" interaction) models the natural tendency of a driver to catch up with the car ahead. Thus clusters of synchronously moving particles or cars may appear, leading to higher throughput (current) in the system. The higher the value of $p_m$ is the more motion of particles in clusters is favored. There are many other systems where aggregation (and fragmentation) of particles into clusters play an important role. Their tendency to aggregate is modelled as attraction interaction. Some of these systems appear in aerosol physics, polymer growth, etc. In living systems the aggregation of pathogenic proteins in the cells may lead to the appearance of a number of neurodegenerative diseases like Alzheimer's, prion diseases, etc. [25]. We would like to point out here that knowledge of behavior and predictions of different simple models of aggregation-fragmentation phenomena could be helpful in understanding better the contributions of specific interactions and processes, playing part in real aggregation phenomena. Though simple, they can still serve as guide for future experiments.

We note that the above generalized backward-ordered dynamics was suggested as exactly solvable one by Wölki [14], and studied on a ring in Refs. [26–28]. The limit case of gTASEP with $p_m = 1$ corresponds to irreversible aggregation, or jam formation in the case of vehicles, suggested and studied by Bunzarova and Pesheva [29] and further elaborated in Refs. [30,31]. Here, we focus on the nonequilibrium stationary properties of gTASEP when $p < p_m < 1$, describing the generic case of attraction between particles, hopping stochastically and unidirectionally in discrete time along finite one-dimensional chains with given boundary conditions at the ends. In particular, we are interested to see how the phase diagram of gTASEP with $p_m = 1$ is destroyed and transformed into a new one when the condition $p_m = 1$ is relaxed to $p < p_m < 1$.

## II. THE MODEL AND SOME KNOWN RESULTS

### A. The model

The dynamics of the gTASEP follows the discrete time backward-sequential rules [20,21], however, modified to include two hopping probabilities: $p$ and $p_m$—see Fig. 1, where a schematic image of gTASEP is presented. Single particles and the first particle of a cluster on the right (called head particle) may move one site to the right with probability $p$. Particles, which belong to a cluster (except the head particle) may move one site to the right, provided the particle in front of them has moved at the same time step, with a modified probability $p_m$. The case when $p_m > p$ models the behaviour of drivers in real traffic to follow the car ahead, thus leading to the appearance of more clusters moving in the system, which in turn leads to higher current.

More precisely, we consider an open one-dimensional lattice of $L$ sites. An occupation number $\tau_i$ is associated with a site $i$, where $\tau_i = 0$, if site $i$ is empty and $\tau_i = 1$, if site $i$ is occupied. During each discrete moment of time $t$, an update of the configuration of the whole chain with $L$ sites, labelled by $i = 1, 2, \ldots, L$, takes place in $L + 1$ steps, passing through successive updates of the right boundary site $i = L$, all the pairs of nearest-neighbor sites in the backward order $(L - 1, L), \ldots, (i, i + 1), \ldots, (1, 2)$, and, finally, the left boundary site $i = 1$ is updated. According to the generalized backward-sequential rules:

(1) Each integer time moment $t$ (or else configuration update) starts with the update of the last site of the chain: if site $i = L$ is occupied, the particle at it leaves the system with probability $\beta$ and stays in place with probability $1 - \beta$. If the last particle has left the system, then if there is a particle at site $i = L - 1$, it moves to the site $i = L$ with modified probability $p_m$; otherwise, it remains immobile with probability $1 - p_m$.

(2) Next, a particle at site $i = 1, 2, \ldots, L-2$ hops to an empty site $i+1$ with probability $p$ or $p_m$, depending on the update of the next nearest neighbor on the right-hand side at the current moment of time. Isolated particles and the first particle of a cluster of particles hop one site forward with probability $p$. When the first particle of a cluster hops, the remaining particles of the same cluster may hop during the same integer-time moment with a modified probability $p_m$, i.e.:

(i) if site $i$ is occupied and site $i+1$ is empty at the beginning of the current update, then the particle from site $i$ jumps to site $i+1$ with probability $p$ and stays immobile with probability $1-p$;

(ii) alternatively, if site $i+1$ is occupied at the beginning of the current moment of time $t$ and became empty after the particle from $i+1$ jumped to the empty $i+2$, then the particle at site $i$ jumps to site $i+1$ with probability $p_m$ and stays immobile with probability $1-p_m$.

(3) The left boundary condition also depends on the occupation history of the right nearest-neighbor. If site $i=1$ was empty at the beginning of the current update, then a particle enters the system with probability $\alpha$ or site $i=1$ remains empty with probability $1-\alpha$. Alternatively, if site $i=1$ was occupied at the beginning of the current moment of time, but became empty under its current update, then a particle enters the chain with probability $\tilde{\alpha}$ or the site remains empty with probability $1-\tilde{\alpha}$. Note, that to ensure consistency with the update rules in the bulk, one needs to set $\tilde{\alpha} = \alpha p_m/p$. However, $\tilde{\alpha}$ (which is a probability) may exceed 1 for some values of the parameters $\alpha$, $p$ and $p_m$, thus one needs to set

$$\tilde{\alpha} = \min\{1, \alpha p_m/p\}. \tag{1}$$

We note that the above left boundary condition was introduced first by Hrabák in Ref. [32] and, independently, in Ref. [29]. It provides also smooth transition of gTASEP to the special cases of the ordinary TASEP with BSU, when $p_m = p$ and $\tilde{\alpha} = \alpha$, as well as to the TASEP with parallel update, when $p_m = 0$ and $\tilde{\alpha} = 0$.

### B. Known results in particular cases

Here we summarize some known results about the phase diagrams and the phase transitions between the stationary phases of gTASEP in the particular cases of $p_m = p$ (the ordinary TASEP with BSU) and $p_m = 1$ (irreversible aggregation). The corresponding phase diagrams are shown in Fig. 2 and density profiles (local density $\rho(x)$ along the chain length) are shown at representative points of the different phases of the respective phase diagrams in Fig. 3.

In Fig. 2(a) the nonequilibrium phase transitions between low-density (LD) phase (LD = AI ∪ AII) and maximum-current (MC) phase, as well as between high-density (HD) phase (HD = BI ∪ BII) and MC phase, are continuous, while the transition between LD and HD is discontinuous, with a finite jump in the local density. The subregions AI (BI) and AII (BII) differ by the shape of the local density profiles [see also Fig. 3(a) below]. The exact critical injection/ejection rate values are $\alpha_c = \beta_c = 1 - \sqrt{1-p}$. In our case of $p = 0.6$, $\alpha_c = \beta_c = 0.367544\ldots$.

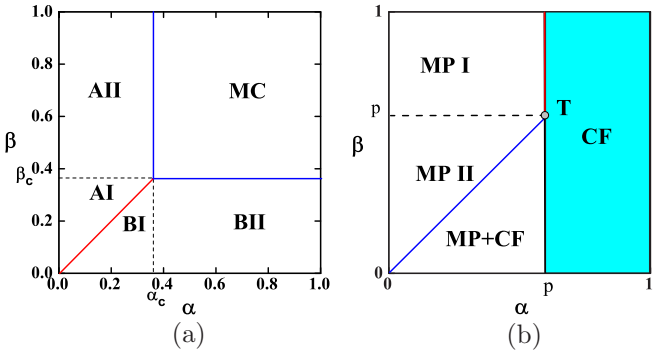


FIG. 2. Phase diagrams in the $\{\alpha, \beta\}$-plane of: (a) the standard TASEP with BSU with $p = p_m = 0.6$. There are three stationary phases: maximum-current phase, MC, low-density phase, LD = AI ∪ AII, and high-density phase, HD = BI ∪ BII; (b) the gTASEP with $p = 0.6$ and $p_m = 1$. The three stationary phases are of different nature: a many-particle phase MP = MPI ∪ MPII, a CF phase of completely filled chains, and a mixed MP+CF phase.

In Fig. 2(b) the many-particle phase MP contains a macroscopic number of particles or clusters of size $O(1)$ as $L \to \infty$; MPI and MPII differ only by the shape of the local density profile [see Fig. 3(b)], which results from the different type of evolution of the configuration gaps. However, in contrast to the case of the standard TASEP, where a similar place in the phase diagram is taken by a LD phase, here the bulk density ($\rho_b = \alpha_b/p$) can take any value from zero to one. In the region MPI, the inequality $\beta > p$ leads to growing average width of the rightmost gap, hence the profile bends downward near the chain length. In the complementary region MPII, the opposite inequality $\beta < p$ holds and the rightmost gap is short-living, while the gaps on the left-hand side of it have a critical type of evolution with mean lifetime of the order $O(L^{1/2})$; see Ref. [31]. The unusual phase transition (found in Ref. [29]) is manifested by the jumps both in the bulk density $\rho_b(\alpha)$ and the current $J(\alpha)$. It takes place across the boundary $\alpha = p$ between the MPI and CF phases.

The phase MP+CF is mixed in the sense that the completely filled configurations are perturbed by short living gaps entering the chain from the first site. The configurations of the stationary nonequilibrium phase CF represent a completely filled chain with current $J = \beta$ [not shown in Fig. 3(b) to avoid overfilling the figure]. If one interprets the probability of completely filled lattice, $P(1)$, as an order parameter, then one has a continuous, clustering type phase transition throughout MP+CF phase, from a completely disaggregated phase in MPII to a completely aggregated one in CF.

## III. THE GENERIC CASE OF ATTRACTION

First, we aim here to analytically approach the question of how the completely filled phase (CF) at $p_m = 1$ [see Fig. 2(b)] is destroyed, when $0 < 1 - p_m \ll 1$, and transformed into new phases typical for $p_m < 1$ [see Fig. 2(a)]. One of the methods, developed in Refs. [30,31], and which is used also here, is based on the study of the time evolution of single gaps in different regions of the CF phase.

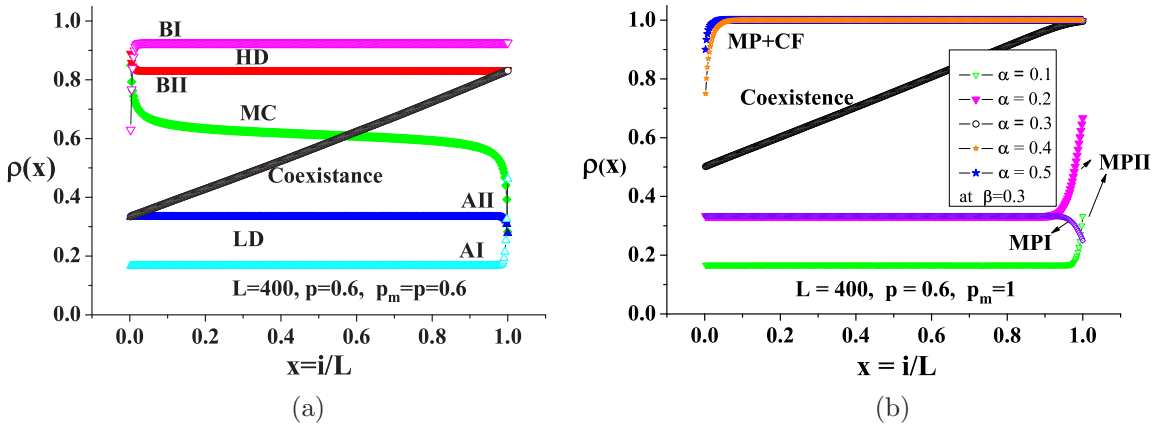


FIG. 3. Typical density profiles (local density $\rho(x)$ as function of space variable $x = i/L$) for a chain of $L = 400$ sites, hopping probability $p = 0.6$, are shown at representative points of the different phases of the respective phase diagrams for: (a) ordinary TASEP with BSU ($p_m = p$): two points in the LD phase, $\alpha = 0.2, \beta = 0.6$ (AII)—solid (blue) down triangles, $\alpha = 0.2, \beta = 0.1$ (AI)—empty (cyan) down triangles; coexistance $\alpha = 0.2, \beta = 0.2$—empty (black) circles; MC phase $\alpha = 0.6, \beta = 0.8$ – solid (green) diamonds, and two points in HD phase, $\alpha = 0.2, \beta = 0.1$ (BI)—empty (magenta) up triangles, $\alpha = 0.6, \beta = 0.2$ (BII)—solid (red) up triangles; and (b) gTASEP in the limit case of irreversible aggregation ($p_m = 1$) at fixed ejection probability $\beta = 0.3$: two values of $\alpha$ from phase MPII: $\alpha = 0.1$—empty (green) down triangles, and $\alpha = 0.2$ – solid (magenta) down triangles, the coexistence line of phases MPII and MP+CF, appearing when $\alpha = \beta = 0.3$—empty (black) circles, and phase MP+CF at $\alpha = 0.4$—empty (orange) stars and $\alpha = 0.5$—solid (blue) stars. A point form MPI phase is shown, appearing when $\alpha = 0.2$ and $\beta = 0.8$—empty (purple) diamonds.

Second, we present results of extensive computer simulations, which suggest the topology of the modified phase diagram, the shift of the triple point $[\alpha_c(p, p_m), \beta_c(p, p_m)]$ under the change of $p_m \in [p, 1]$ at fixed $p$, and the nature of the phase transitions between the stationary nonequilibrium phases.

### A. Time evolution of configuration gaps

We begin with finding out the probability of a single gap appearance under boundary conditions corresponding to the CF phase. Then we consider the first step in the time evolution of the gap width. The problem is rather complicated because the probability of appearance of a gap is position dependent when $p_m < 1$. In contrast to the case of $p_m = 1$, here we show that when $\beta \neq p$, the gap width performs a special, position dependent random walk.

Let $P_i(p, p_m)$ denote the probability of appearance of a single gap at site $i = 1, 2, \ldots, L$ in a completely filled configuration with $\tau_1 = \tau_2 = \ldots \tau_L = 1$, when $0 < 1 - p_m \ll 1$. For brevity of notation, we do not show the explicit dependence on the injection and ejection rates of that probability. Since we exclude the appearance of a second gap, under the generalized backward-sequential update we obtain

$$P_{L-k}(p, p_m) = (1 - p_m)p_m^k\beta,\ k = 0, 1, \ldots L - 2,$$
$$P_1(p, p_m) = (1 - \tilde{\alpha})p_m^{L-1}\beta. \tag{2}$$

Under the assumption $0 < 1 - p_m \ll 1$, the left boundary condition yields $\tilde{\alpha} = 1$ for all $p < \alpha \leqslant 1$, which means that $P_1(p, p_m) = 0$ at the beginning of each update. Therefore, we focus on the case when the gap appears at sites $2 \leqslant i \leqslant L$. Then, the right edge of the gap, positioned at site $i + 1 < L$ can move one site to the right, provided that site is empty. The latter event occurs only if the particle at site $i = L$ leaves the system with probability $\beta$, and the remaining cluster of $L - i - 1$ particles at sites $i + 1, \ldots, L - 1$ moves as a whole entity one site to the right, which happens with probability $p_m^{L-i-1}$. Thus, the total probability for the particle at the right edge to hop to the right is $p_m^{L-i-1}\beta$, and to remain at its place is $(1 - \beta) + (1 - p_m^{L-i-1})\beta$. However, the particle at the left edge $i - 1$, being either the rightmost particle of a cluster or isolated, may hop to the right with the position independent probability $p$, and stay immobile with probability $1 - p$. As a result, the gap width increases by one site with probability

$$p_g(i) = (1 - p)p_m^{L-i-1}\beta, \tag{3}$$

decreases by one site with probability

$$q_g(i) = \big[(1 - \beta) + \big(1 - p_m^{L-i-1}\big)\beta\big]p = \big(1 - p_m^{L-i-1}\beta\big)p, \tag{4}$$

and remains the same with probability

$$r_g(i) = 1 - p + p_m^{L-i-1}\beta(2p - 1). \tag{5}$$

As expected, at $p_m = 1$ these expressions reduce to equalities Eq. (4) in Ref. [31]. As is readily seen, in the alternative case of several coexisting gaps, the above probabilities apply exactly to the rightmost one.

Now we have to average the gap width evolution over the initial probabilities given by Eq. (2). The probability normalization factor under the condition of a single gap opened at sites $i = 2, 3, \ldots, L$ is

$$N(p, p_m) = (1 - p_m)\beta\sum_{k=0}^{L-2} p_m^k = \beta\big(1 - p_m^{L-1}\big). \tag{6}$$

Then, the changes in the gap width at the first time step, averaged over all events of gap appearance at sites $i = 2, 3, \ldots, L$, become as follows:

The gap width increases by one site with probability

$$\bar{p}_g = \frac{(1-p)(1-p_m)\beta}{p_m\left(1-p_m^{L-1}\right)} \sum_{k=2}^{L} p_m^{2k} = \frac{(1-p)\left(1+p_m^{L-1}\right)\beta}{p_m(1+p_m)}, \tag{7}$$

decreases by one site with probability

$$\bar{q}_g = \frac{p(1-p_m)}{\left(1-p_m^{L-1}\right)} \sum_{k=0}^{L-2} \left(p_m^k - p_m^{2k-1}\beta\right) = p - \frac{p\left(1+p_m^{L-1}\right)\beta}{p_m(1+p_m)}, \tag{8}$$

and remains the same with probability

$$\begin{aligned}\bar{r}_g &= \frac{(1-p_m)}{\left(1-p_m^{L-1}\right)} \sum_{k=0}^{L-2} \left[(1-p)p_m^k + p_m^{2k-1}\beta(2p-1)\right] \\ &= 1 - p + \frac{(2p-1)\beta\left(1+p_m^{L-1}\right)}{p_m(1+p_m)}. \end{aligned} \tag{9}$$

Notably, at $p_m = 1$ the above results reduce again to equalities Eq. (4) in Ref. [31].

By comparing the expressions for $\bar{p}_g$ and $\bar{q}_g$, we conclude that on the average a single-site gap will grow after the first time step of its evolution when

$$\beta > p\frac{p_m(1+p_m)}{\left(1+p_m^{L-1}\right)}. \tag{10}$$

When $p_m \to 1$ and $L$ is fixed, or $L \to \infty$ so that $p_m^L \to 1$, this condition simplifies to $\beta > p$. However, for fixed values of $p_m$ close to 1, $p_m^L$ will decrease to zero as $L \to \infty$. For example, in our computer simulations we used: $p_m = 0.99$ and $L = 800$, which yields $p_m^{L-1} \simeq 3.22 \times 10^{-4}$ and the criterion becomes much stronger, $\beta > 1.97p$. However, with each time step $j = 1, 2, \ldots$ the right edge of the gap will hop forward by one site with increasing probability $p_m^{L-i-j}\beta$, while its left edge may hop to the right with the position independent probability $p$. Thus, the value of $p_g(i)$ will increase and the value of $q_g(i)$ will decrease in the course of time.

Without going into the involved details of the complete gaps evolution, we conjecture that the simple criteria $\beta > p$ for growing gaps, and $\beta < p$ for decreasing gaps, hold true. Thus, our expectation, confirmed by the computer simulations, is that in the upper region $(p < \alpha \leqslant 1] \times (p < \beta \leqslant 1]$ of the CF phase a maximum-current phase will appear. Its local density profile satisfies the inequalities $\rho_1 = 1 > \rho_{l/2} > \rho_L$, which follow from the conditions $\tilde{\alpha} = 1$, and the larger probability of gap formation near the end of the chain. In the lower region $(p < \alpha \leqslant 1] \times (0 < \beta < p]$ of the CF phase the gaps are scarce, small and short-living, which is indicative of a high-density phase. Again, the left-hand side of the local density profile bends upward to $\rho_1 = 1$.

Note that in the above consideration $p = \lim_{p_m \to 1-0} \sigma_c(p, p_m)$. In the case of $p_m < 1$, the critical values should decrease down to $\sigma_c(p, p) = 1 - \sqrt{1-p}$, as $p_m \to p + 0$.

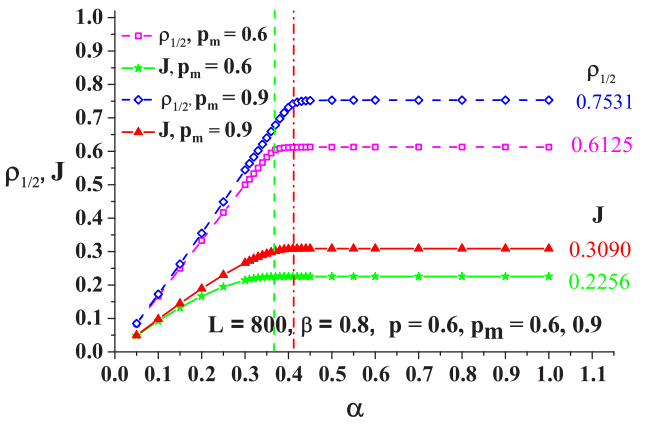


FIG. 4. Behavior of the stationary midpoint density, $\rho_{1/2}$, and the current, $J$, for the gTASEP for two values of the modified hopping probability, $p_m = 0.6$ and $p_m = 0.9$, as a function of the input rate $\alpha$ at chain length $L = 800$ sites, fixed $p = 0.6$ and output rate $\beta = 0.8$. Apparently, their behavior (for $p_m = 0.6$ and for $p_m = 0.9$) is similar and reflects the continuous nonequilibrium phase transition across the segment $\beta_c(p, p_m) < \beta \leqslant 1$, however, with different, $p_m$-dependent critical values: our estimates for $p_m = 0.9$ are $\alpha_c(0.6, 0.9) = \beta_c(0.6, 0.9) \simeq 0.41$ ($\alpha_c(0.6, 0.9)$ is shown by the vertical red dashed-dotted line). The vertical green dashed line shows the position of the critical value $\alpha_c(0.6, 0.6) = 0.367544$ of the ordinary TASEP with backward sequential update.

### B. Phase diagram and phase transitions

We performed Monte Carlo simulations of the gTASEP on open chains of mainly $L = 800$ and $L = 1600$ sites. Each run started with $10^6$ relaxation updates and had not less than $10^4$ attempted updates per lattice site. The stationary properties were evaluated by averaging over 100 (quasi)independent runs. The estimated accuracy is $O(10^{-3})$ for the local particle density and $O(10^{-4})$ for the current.

First, we compare the behavior of the current, $J$, and the local density at the midpoint of the chain, $\rho_{1/2}$, under two modified hopping probabilities $p_m = 0.6$ and $p_m = 0.9$, as a function of the input rate $\alpha$, at chain length $L = 800$ sites, fixed $p = 0.6$ and output rate $\beta = 0.8$; see Fig. 4.

We recall that in the standard backward-sequential TASEP with $p = 0.6$, the exact results in the thermodynamic limit $L \to \infty$ are: for the critical injection/ejection values

$$\alpha_c = \beta_c = 1 - \sqrt{1-p} = 0.367544\ldots,$$

for the current in the maximum-current phase

$$J^{\mathrm{MC}} = \frac{1-\sqrt{1-p}}{1+\sqrt{1-p}} = 0.225148\ldots,$$

and for the midpoint density in the MC phase

$$\rho_{1/2}^{\mathrm{MC}} = \frac{1}{1+\sqrt{1-p}} = 0.612574\ldots.$$

The critical value $\alpha_c$, shown in Fig. 4 by a vertical green dashed line, corresponds to the transition of the asymptotic behavior of the current $J$ (at $p_m = 0.6$) near $\alpha_c$ from a parabolic one on the left-hand side of the segment $\beta_c(0.6, 0.6) < \beta \leqslant 1$, to a constant value in the MC phase on the right-hand side of

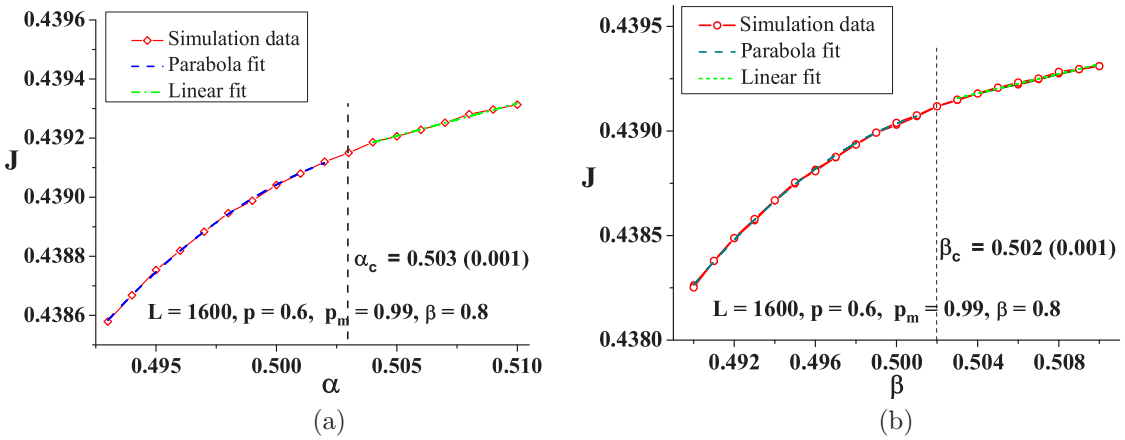


FIG. 5. The current in the gTASEP when $p = 0.6$, $p_m = 0.99$ and $L = 1600$ sites, as a function of: (a) the injection probability $\alpha$ (at $\beta = 0.8$). The critical value $\alpha_c(0.6, 0.99) = 0.503 \pm 0.001$ is estimated from the apparent change in the asymptotic behavior of the current; (b) the ejection probability $\beta$ (at $\alpha = 0.8$). The critical value $\beta_c(0.6, 0.99) = 0.502 \pm 0.001$ is estimated from the apparent change in the asymptotic behavior of the current.

it. Due to finite-size effects, the current $J^{\rm MC}$ slightly grows with $\alpha$ up to 0.2256 at $\alpha = 1$.

Similarly, at $p_m = 0.9$, we see that the phase transition across the segment $\beta_c(0.6, 0.9) < \beta \leqslant 1$ is continuous too and we estimate the critical values $\alpha_c(0.6, 0.9) = \beta_c(0.6, 0.9) \simeq 0.41$, see the vertical red dash-dotted line in Fig. 4. This indicates that the unusual phase transition, found in [29] at $p_m = 1$ across the boundary $\alpha = p$ becomes a continuous one. Note that in the MC phase the current grows up to $J^{\rm MC}(0.6, 0.9) = 0.3090\ldots$ and the local density $\rho^{\rm MC}_{1/2}(0.6, 0.9)$ up to 0.7531.

To check the continuity of the phase transition across the segment $\beta_c < \beta \leqslant 1$, we consider in more detail both the $\alpha$- and $\beta$-dependence of the current on larger lattice and value of $p_m$ closer to 1, namely $L = 1600$ and $p_m = 0.99$. The results are shown in Figs. 5(a) and 5(b).

It is instructive to analytically check the above estimates for the critical values of the injection (ejection) $\alpha_c$ ($\beta_c$) probabilities, commonly denoted by $\sigma_c$. To this end we use the continuity condition for the first derivative of the current: $J'(\sigma_c - 0) = J'(\sigma_c + 0)$. Close to the critical value $\sigma_c$, we have a parabolic approximation for the current below $\sigma_c$,

$$J(\sigma < \sigma_c) = A + B\sigma + C\sigma^2, \tag{11}$$

and a linear approximation above $\sigma_c$,

$$J(\sigma > \sigma_c) = a + k\sigma. \tag{12}$$

Hence, in the case of a continuous second order phase transition, when $J'(\sigma_c - 0) = J'(\sigma_c + 0)$, we obtain an estimate for $\sigma_c$:

$$\sigma_c = \frac{k - B}{2C}. \tag{13}$$

In the case of the current as a function of $\alpha$, see Fig. 5(a), the best least-square fit yields

$$A = -0.386 \pm 0.05, \quad B = 3.229 \pm 0.21,$$
$$C = -3.186 \pm 0.21, \quad k = 0.022 \pm 7.7 \times 10^{-4}, \tag{14}$$

which leads to the estimate $\alpha_c = 0.503 \pm 0.07$. In spite of the large error interval, this estimate coincides with our former value of $\alpha_c(0.6, 0.99) \simeq 0.503$.

In the complementary case of the $\beta$-dependent current, see Fig. 5(b), the best least-square fit yields

$$A = -0.536 \pm 0.055, \quad B = 3.86 \pm 0.22,$$
$$C = -3.82 \pm 0.22, \quad k = 0.023 \pm 0.001, \tag{15}$$

which leads to the estimate $\beta_c = 0.502 \pm 0.05$. Again, the error bars are rather large, but this estimated value also coincides with our former assessment of $\beta_c(0.6, 0.99) \simeq 0.502$. Finally, we assume that within error bars $\alpha_c(0.6, 0.99) = \beta_c(0.6, 0.99) = 0.502 \pm 0.02$.

Now we focus on the phase transitions taking place by changing $\alpha$ across the segment $0 < \beta < \beta_c(p, p_m)$. In Ref. [29], a mixed MP+CF phase was found at $p_m = 1$, see Fig. 2(b). This phase is characterized by the nonzero probability $P(1)$ of appearance of a cluster spanning the whole chain of $L$ sites: $P(1)$ changes with $\alpha$ from zero at the left phase boundary $0 < \alpha = \beta < p$ to $P(1) = 1$ at the right boundary $\alpha = p$, $0 < \beta < p$ with the CF phase. In Ref. [31] the MP+CF phase was interpreted as a boundary perturbed one. Here we show that as $p_m < 1$, $P(1)$ exponentially decreases to zero, not only in the MP+CF phase but also in the subregion $(0 < \alpha < \alpha_c) \times (0 < \beta < \beta_c)$, which at $p_m = 1$ belongs to the CF phase. The results of our computer simulations for the cluster-size distribution in gTASEP when $p_m = 0.99$ at $\alpha = 0.6$, $\beta = 0.25$, and lattice sizes $L = 200, 400, 800$ are shown in Fig. 6.

By using a larger series of chain sizes, from $L = 200$ to $L = 1600$, we obtain that $P(1)$ probability decays exponentially fast with the unlimited increase of $L$,

$$P_L(1) \simeq 0.2426 \times \exp\{-(L - 200)/140\}, \quad L \geqslant 200. \tag{16}$$

The quality of the fit is illustrated in Fig. 7.

Therefore, by continuity arguments, we conclude that in the thermodynamic limit $L \to \infty$ the regions between the left-hand boundary $0 < \alpha = \beta < \sigma_c(p, p_m)$ and the right-hand boundary at $\alpha = 1$ and $0 < \beta < \beta_c(p, p_m)$, belong to the

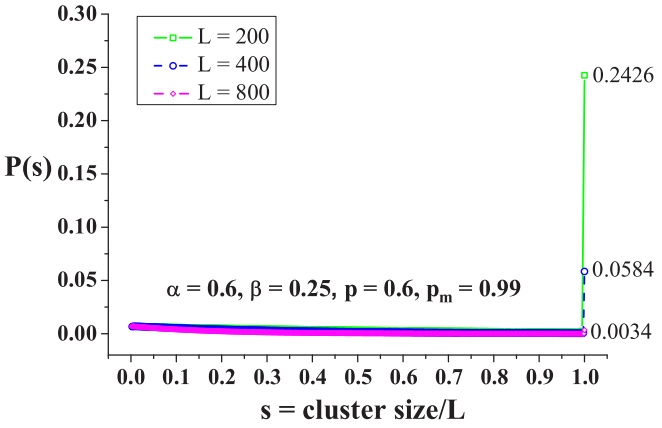


FIG. 6. Cluster size distribution in the gTASEP when $p = 0.6$, $p_m = 0.99$ on lattices $L = 200, 400, 800$ sites at $\alpha = 0.6$, and $\beta = 0.25$. At $L = 1600$ the estimated value of $P(1)$ drops down to $1.147 \times 10^{-5}$.

same phase. The fact that across the coexistence line $0 < \alpha = \beta < \sigma_c(p, p_m)$ there occurs a first-order phase transition is seen from the shape of the local density profiles, shown in Fig. 8 at different points $(\alpha, \beta)$ in the $\alpha$-$\beta$ plane.

By using continuity arguments, we generalize the above results to conjecture a generic phase diagram of the gTASEP with $p_m < 1$ with the same topology as in the case of the backward-sequential TASEP, see Fig. 2(a), but with $(p, p_m)$-dependent triple point $(\alpha_c, \beta_c)$. In Fig. 9 we exemplify the phase diagram of the gTASEP in the particular case of $p = 0.6$ and $p_m = 0.99$ and the shift of the triple point $(\alpha_c, \beta_c)$ with the increase of $p_m$ at fixed $p = 0.6$.

Now one can see the similarity in the behavior of the local density profiles in the cases $p_m = p < 1$ and $p < p_m < 1$. In the low-density phase LD = LDI ∪ LDII the bulk density is less than $1/2$, the difference between the LDI and LDII regions is in the right-hand end of the local density profile: in LDI it bends upward, while in LDII it bends downward, similarly to the case of the standard backward-sequential TASEP. This can be readily explained by using the exact relationship

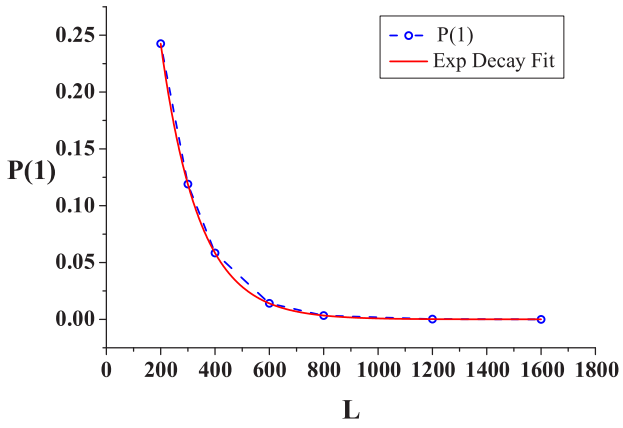


FIG. 7. Least-square fit to the exponential decay of the complete-cluster probability $P(1)$ with the unlimited increase of the chain length $L$ in the gTASEP when $p = 0.6$ and $p_m = 0.99$ at $\alpha = 0.6$ and $\beta = 0.25$.

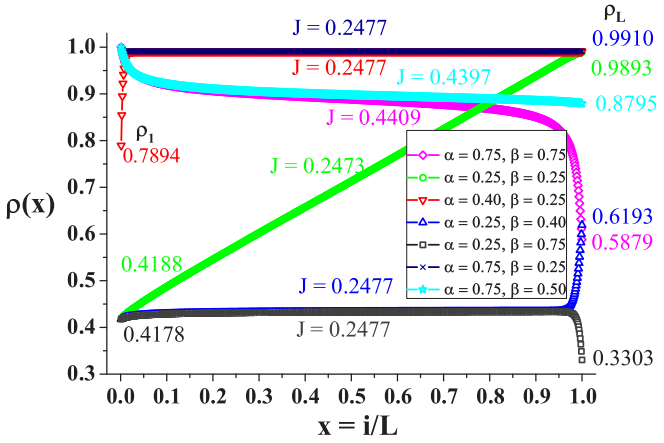


FIG. 8. Local density profiles of the gTASEP when $p = 0.6$ and $p_m = 0.99$ at different points in the phase space. Obviously, the point $(\alpha = 0.25, \beta = 0.25)$ lies on the coexistence line between the low-density phase, represented by the points $(\alpha = 0.25, \beta = 0.40)$ and $(\alpha = 0.25, \beta = 0.75)$, and the high-density phase, represented by the points $(\alpha = 0.40, \beta = 0.25)$, $(\alpha = 0.75, \beta = 0.25)$, and $(\alpha = 0.75, \beta = 0.50)$. The corresponding value of the current $J$ is denoted next to every density profile.

$\rho_L = J/\beta$, and assuming the same value of the current in the two regions. In the considered particular case of $p = 0.6$ and $p_m = 0.99$, the bulk density in the high-density phase is very close to 1, the difference between the regions HDI and HDII being at left-hand side of the profile: In HDI it sharply bends downward, while in HDII it bends upward, again similarly to the case of the standard backward-sequential TASEP.

Additional information can be found in the different gaps evolution regimes in regions LDI and HDI: in both cases

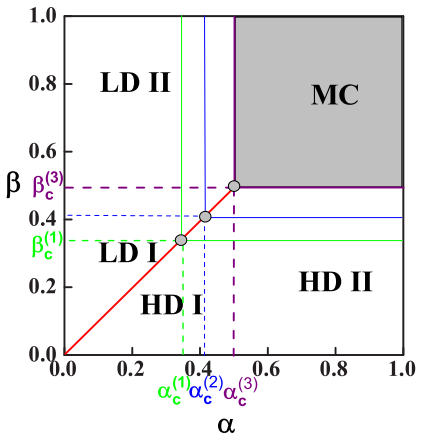


FIG. 9. Conjectured phase diagram of the gTASEP when $p = 0.6$ and $p_m = 0.99$ (purple lines). It has the same topology as in the case of the standard TASEP with backward-sequential update [shown in Fig. 1(a)], but with different, $p_m$-dependent critical values—our estimates are $\alpha_c^{(3)}(0.6; 0.99) = \beta_c^{(3)}(0.6; 0.99) = 0.502$, see text. To illustrate the shift of the triple point we have added also the critical lines of the standard backward sequential TASEP, i.e., $\alpha_c^{(1)}(0.6; 0.6) = \beta_c^{(1)}(0.6; 0.6) = 0.3675$ (thin green lines) and of the gTASEP with $p = 0.6$ and $p_m = 0.9$ – $\alpha_c^{(2)}(0.6; 0.9) = \beta_c^2(0.6; 0.9) = 0.41$ (thin blue lines).

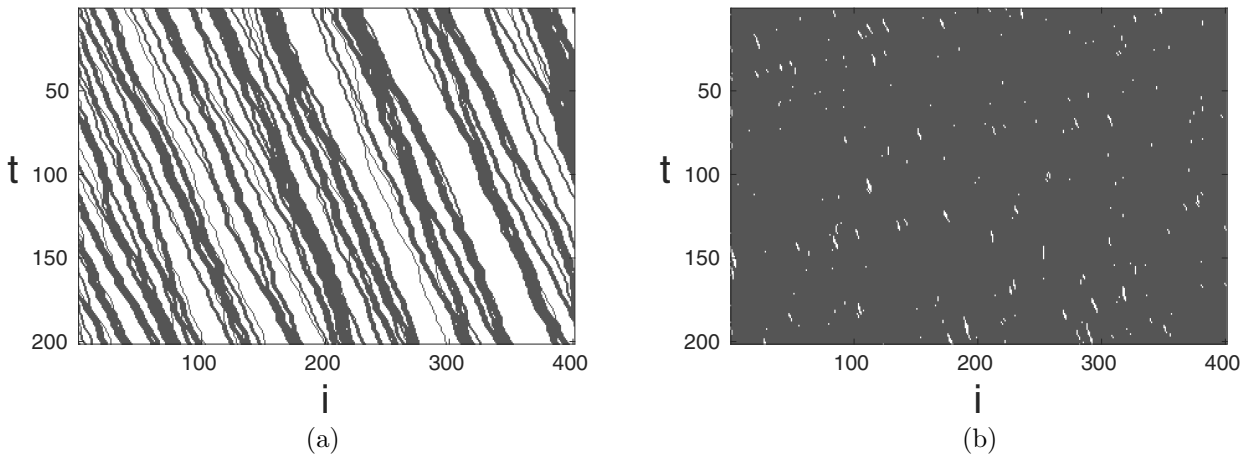


FIG. 10. A space-time plot (time is flowing downward in the vertical direction) of the gTASEP when $p = 0.6$, $p_m = 0.99$, and $L = 400$ sites, showing the gaps evolution, in: (a) region LDI ($\alpha = 0.25$, $\beta = 0.40$)—white stripes; (b) in region HDI ($\alpha = 0.40$, $\beta = 0.25$)—white spots.

$\alpha < p$, which implies $\tilde{\alpha} < 1$, so that gaps can appear at the first site $i = 1$ and evolve throughout the chain; however, in LDI the gaps are wide and long-living, while in HDI they are small, scarce and very short living, compare Figs. 10(a) and 10(b). The typical gaps pattern in LDII (HDII) is similar to the one shown for LDI (HDI). These features may explain the large difference in the particle densities in the low-density and high-density phases.

Here we emphasize that the gTASEP does not satisfy the particle-hole symmetry inherent to the standard versions of TASEP. For example, the fundamental diagram of the generic model, obtained by Hrabák, see Fig. 6.2 in Ref. [32], where $\gamma = p_m/p$, is not symmetric under the replacement $\rho \leftrightarrow 1 - \rho$. The above mentioned phase diagram was obtained in the thermodynamic limit under periodic boundary conditions, which means that the very bulk dynamics at $p < p_m$ does not respect the particle-hole symmetry. In addition, in our case of open boundaries, the left boundary condition Eq. (1) is not appropriate for introduction of holes from the right chain end. Therefore, it is rather unexpected that the currents in the phases LD and HD, calculated at symmetric points $(\alpha, \beta)$ and $(\beta, \alpha)$, are equal: $J^{\mathrm{LD}}(\alpha = 0.25, \beta = 0.75) = J^{\mathrm{HD}}(\alpha = 0.75, \beta = 0.25) \simeq 0.2477$.

## IV. DISCUSSION

We studied the generalized TASEP in the regime of particle attraction ($p_m > p$) between hopping nearest-neighboring particles. In this case ($p < p_m < 1$) cluster aggregation and fragmentation is allowed in the system. A central problem of interest was to find how the topology of the phase diagram in the case of irreversible aggregation $p_m = 1$, see Fig. 2(b), transforms into the topology of the well-known phase diagram of the usual TASEP with backward-ordered sequential update, see Fig. 2(a), when $p_m$ decreases from $p_m = 1$ down to $p_m = p$. Based on an incomplete random-walk theory and on extensive Monte Carlo calculations, we conjectured that the above phenomenon takes place sharply, as soon as $p_m$ becomes less than 1. The main difference between the phase diagrams for $p_m = 1$ and $p_m < 1$ turned out to be the dependence of the critical probabilities $\sigma_c(p, p_m)$ on $p_m$, at fixed $p$. Apart from that, we have shown the similarity of the local density profiles and the current as a function of the injection $\alpha$ and ejection $\beta$ probabilities, in the cases $p_m = p$ and $p_m > p$. The main effect of increasing the modified hopping probability $p_m$ turns out to be increase in the values of critical point coordinates, the bulk density and the current. For example, on passing from $p_m = p$ to $p_m = 0.99$, these values grow from

$$\alpha_c = \beta_c \simeq 0.3675, \quad J^{\mathrm{MC}} \simeq 0.2251, \quad \rho_{1/2}^{\mathrm{MC}} \simeq 0.6126,$$

to

$$\alpha_c = \beta_c \simeq 0.502, \quad J^{\mathrm{MC}} \simeq 0.4409, \quad \rho_{1/2}^{\mathrm{MC}} \simeq 0.8891.$$

On the ground of our random walk theory and the computer simulations, we have conjectured that the simple criteria $\beta > p$, for growing gaps, and $\beta < p$, for decreasing gaps, hold true on the average.

An interesting result is the exponential decay to zero of the probability $P(1)$ of a complete cluster in the HDII phase (which emerges in the lower region of the CF phase of the gTASEP with $p_m = 1$), when $p_m < 1$ and the chain length $L$ increases unboundedly; see Fig. 7.

There are still many open problems, such as an elaboration of the random walk theory to the extent of yielding both qualitative and quantitative predictions, the analytical derivation of the local density at the chain ends, and the value of the current in the different stationary phases, just to mention a few.

## ACKNOWLEDGMENTS

The authors gratefully acknowledge the fruitful discussions with their late colleague and coauthor, Professor V. B. Priezzhev, held at an early stage of the present study. This work has been accomplished with the financial support of the Bulgarian MES by Grant No. D01-221/03.12.2018 for NCDSC—part of the Bulgarian National Roadmap on RIs.

[1] B. Derrida, Phys. Rep. **301**, 65 (1998).
[2] G. M. Schütz, in *Phase Transitions and Critical Phenomena*, edited by C. Domb and J. L. Lebowitz, Vol. 19 (Academic Press, London, 2001), pp. 1–251.
[3] K. Mallick, J. Stat. Mech. (2011) P01024.
[4] C. T. MacDonald, J. H. Gibbs, and A. C. Pipkin, Biopolymers **6**, 1 (1968).
[5] F. Zhang, C. L. Liu, and B. R. Hu, J. Neurochem. **98**, 102 (2006).
[6] T. Tripathi and D. Chowdhury, Phys. Rev. E **77**, 011921 (2008).
[7] P. Greulich, A. Garai, K. Nishinari, A. Schadschneider, and D. Chowdhury, Phys. Rev. E **75**, 041905 (2007).
[8] A. B. Kolomeisky, Phys. Rev. Lett. **98**, 048105 (2007).
[9] A. Zilman, J. Pearson, and G. Bel, Phys. Rev. Lett. **103**, 128103 (2009).
[10] K. Nagle, Phys. Rev. E **53**, 4655 (1996).
[11] D. Chowdhury, L. Santen, and A. Schadschneider, Phys. Rep. **329**, 199 (2000).
[12] C. Arita, M. E. Foulaadvand, and L. Santen, Phys. Rev. E **95**, 032108 (2017).
[13] D. Helbing, Rev. Mod. Phys. **73**, 1067 (2001).
[14] M. Wölki, Steady States of Discrete Mass Transport Models, Master thesis, University of Duisburg-Essen, 2005.
[15] B. Derrida, E. Domany, and D. Mukamel, J. Stat. Phys. **69**, 667 (1992).
[16] G. M. Schütz and E. Domany, J. Stat. Phys. **72**, 277 (1993).
[17] B. Derrida, M. R. Evans, V. Hakim, and V. Pasquier, J. Phys. A **26**, 1493 (1993).
[18] H. Hinrichsen, J. Phys. A **29**, 3659 (1996).
[19] A. Honecker and I. Peschel, J. Stat. Phys. **88**, 319 (1997).
[20] N. Rajewski, A. Schadschneider, and M. Schreckenberg, J. Phys. A **29**, L305 (1996).
[21] N. Rajewski and M. Schreckenberg, Physica A **245**, 139 (1997).
[22] M. R. Evans, N. Rajewsky, and E. R. Speer, J. Stat. Phys. **95**, 45 (1999).
[23] J. de Gier and B. Nienhuis, Phys. Rev. E **59**, 4899 (1999).
[24] N. Rajewsky, L. Santen, A. Schadschneider, and M. Schreckenberg, J. Stat. Phys. **92**, 151 (1998).
[25] J. P. Taylor, J. Hardy, and K. H. Fischbeck, Science **296**, 1991 (2002).
[26] A. E. Derbyshev, S. S. Poghosyan, A. M. Povolotsky, and V. B. Priezzhev, J. Stat. Mech. (2012) P05014.
[27] A. E. Derbyshev, A. M. Povolotsky, and V. B. Priezzhev, Phys. Rev. E **91**, 022125 (2015).
[28] B. L. Aneva and J. G. Brankov, Phys. Rev. E **94**, 022138 (2016).
[29] N. Zh. Bunzarova and N. C. Pesheva, Phys. Rev. E **95**, 052105 (2017).
[30] N. Zh. Bunzarova, N. C. Pesheva, V. B. Priezzhev, and J. G. Brankov, J. Phys: Conf. Series **936**, 012026 (2017).
[31] J. G. Brankov, N. Zh. Bunzarova, N. C. Pesheva, and V. B. Priezzhev, Physica A **494**, 340 (2018).
[32] P. Hrabák, Ph.D. Thesis, Czech Technical University in Prague, Faculty of Nuclear Sciences and Physical Engineering, Praga (2014).